Chemical Physics Letters 754 (2020) 137654

Contents lists available at ScienceDirect

Chemical Physics Letters

journal homepage: www.elsevier.com/locate/cplett

Research paper

Calculations of electron transfer in the tris[4-(2-thienyl)phenyl]amine–C_{70} donor-acceptor system

Titus-Adrian Beu[a,*], Attila Bende[b], Alex-Adrian Farcaş[a,b]

[a] Babeş-Bolyai University, Faculty of Physics, Dept. of Biomolecular Physics, 1 MihailKogălniceanu str., RO-400084 Cluj-Napoca, Romania
[b] National Institute for Research and Development of Isotopic and Molecular Technologies, 67-103 Donath str., RO-400293 Cluj-Napoca, Romania

HIGHLIGHTS

- Electron transfer calculations in the tris[4-(2-thienyl)phenyl]amine–C70 donor-acceptor system.
- Quantum mechanical time-dependent formalism for electronic polpulation evolution.
- Hamiltonian compiled from static DFT calculations and Gaussian perturbation pulse.
- Electron transfer correlated with geometric donor-acceptor configuration, electronic structure, and pulse features.

ARTICLE INFO

Keywords:
Electron transfer
Bulk heterojunction
Donor-acceptor
Fullerene
Photovoltaics

ABSTRACT

The reported work aims to provide new insights into the process of electron transfer in donor-acceptor complexes, of interest for photovoltaic systems based on bulk heterojunctions. Specifically, the star-shaped molecule Tris[4-(2-thienyl)phenyl]amine ($C_{30}H_{21}NS_3$) is considered as donor in combination with the C_{70} fullerene, as acceptor. The electron transfer induced by Gaussian pulses is investigated for several donor-acceptor configurations, with the electronic states described in the framework of a quantum time evolution formalism based on the Cayley propagator. The electron transfer is correlated with the geometric/electronic features of the complexes, as well as the pulse parameters, suggesting optimal setups for practical realizations.

1. Introduction

Photo-induced electron transfer (ET) is a fundamental process in many photochemical applications, such as photovoltaics [1]. Solar cells are generically subdivided into perovskite solar cells, dye-sensitized solar cell materials, and organic photovoltaic (OPV) materials [2]. Even though their efficiency is not yet comparable with that of conventional solar cells, the OPV materials stand out by reduced weight, mechanical flexibility, versatile/low-cost fabrication, and integrability with various other materials. Their main intrinsic limitation, i.e. the low charge carrier (exciton) mobility, is partly compensated by their relatively high UV light absorption coefficients.

The performance of the solar cells is strongly influenced by the initial design of the donor and acceptor materials [3]. Bulk heterojunctions (BHJs) rank among the most frequent implementations of OPV cells, in which the photo-induced ET typically takes place from a π-conjugated polymeric donor to a fullerene-based acceptor, the complex being aggregated by van der Waals interactions [4–8]. Interestingly, free charge carriers can be induced either by the photoexcitation of the electron-accepting molecule (A) or by the photoexcitation of the electron-donating molecule (D). In both cases the positive and negative charges are separated on the neighboring D and A molecules due to photoinduced electron transfer. On the other hand, from a practical and theoretical standpoint, key factors in optimizing the ET process are the geometrical donor-acceptor configuration and the relative position with respect to their neighbors.

Most of the theoretical estimations of the ET process efficiency are based on Marcus semiclassical electron-transfer theory [1,9,10] or on TDDFT calculations [11], but only in few cases the explicit time dependence of the electron transfer dynamics was taken into account [12]. Based on the quantum evolution framework proposed by Allen and co-workers [13] and the formulation developed by Acocella et al. [14], Höfinger et al. [15] reported a first systematic ET study induced by an external field for a good range of C_{60}-based donor-acceptor combinations forming BHJs only quite recently, overcoming significant technical difficulties associated with the intensive underlying

* Corresponding author.
E-mail address: titus.beu@phys.ubbcluj.ro (T.-A. Beu).

https://doi.org/10.1016/j.cplett.2020.137654
Received 8 March 2020; Received in revised form 25 May 2020; Accepted 26 May 2020
Available online 28 May 2020

computations. Very recently, Acocella et al. [16] also investigated ET for terthiophene-C_{60}, a typical dyad with covalently linked donor-acceptor moieties.

The reported study, focuses on Tris[4-(2-thienyl)phenyl]amine ($C_{30}H_{21}NS_3$), as electron donor, and the C_{70} fullerene, as electron acceptor, which have proven to form an effective donor-acceptor pair [17,18]. Notably, the enhanced light absorbing capacity of C_{70} is generally expected to lead to higher cell efficiencies than for C_{60} [19].

The electron dynamics within a time-dependent quantum mechanical framework similar to the one proposed by Acocella et al. [14,15,16], is modelled by using the Cayley's form of the time evolution operator. The employed Hamiltonian combined an adiabatic all-electron part and a periodic Gaussian perturbation. Both the adiabatic part of the Hamiltonian and the initial electronic configuration of the donor-acceptor complex were compiled from static DFT calculations.

The aim of the present paper is to describe the behavior of the mentioned complex under the influence of Gaussian pulses, comparatively investigating the efficiency of the ET for five representative donor-acceptor configurations.

2. Theoretical and computational details

The time evolution of the molecular orbitals (MOs) of the donor-acceptor system is central in describing the ET within the complex. The step-by-step propagation of the one-electron MO Φ_j can be conveniently accomplished by using Cayley's scheme

$$\Phi_j(r, t + \Delta t) = \left(1 + \frac{i\Delta t}{2\hbar}H\right)^{-1}\left(1 - \frac{i\Delta t}{2\hbar}H\right)\Phi_j(r, t), \tag{1}$$

where H is the Hamiltonian, Δt the time step, $\hbar = h/2\pi$ Planck's constant, and i the imaginary unit [20]. Besides being time-reversible, which beneficially translates into numerical stability, this scheme is particularly useful for perturbative Hamiltonians [21,22].

Considering the MOs to be expanded relative to an *orthogonal basis set*, the propagation relation can be actually expressed in terms of the MO *coefficients*, which, rearranged to emphasize the real and imaginary parts for the convenience of actual computations, takes the form:

$$C^{'}(t + \Delta t) = \left[I + \left(\frac{\Delta t}{2\hbar}H\right)^2\right]^{-1}\left\{\left[I - \left(\frac{\Delta t}{2\hbar}H\right)^2\right] - 2i\left(\frac{\Delta t}{2\hbar}H\right)\right\}C^{'}(t) \tag{2}$$

The time evolution of the donor-acceptor system can be modeled by a perturbed Hamiltonian matrix $H = H(t)$, composed of a static part H_0, adiabatically accounting for the (initial) electronic structure of the complex, and a periodic external excitation:

$$H(t) = H_0 - ME_0A(t)\sin(\omega t) \tag{3}$$

where M is the molecular multipole matrix, E_0 is the electric field intensity, and ω is the perturbation frequency. Specifically, in the present investigations we implemented Gaussian perturbation pulses of modulating amplitude

$$A(t) = e^{-(t-\tau)^2/2(\tau/4)^2}. \tag{4}$$

In using the propagation scheme (2) in concrete applications, two major pieces of information need to be provided: (a) the adiabatic Hamiltonian H_0 of the entire donor-acceptor complex, and (b) the initial electronic state of the *non-interacting* complex, expressed through the initial orthogonal MO coefficients, $C^{'}(t = 0)$.

The adiabatic Hamiltonian H_0 can be compiled from elements produced in a standard static first-principles calculation on the donor-acceptor complex, i.e. the one-electron energies ε, the MO coefficients C_0 relative to the employed *non-orthogonal basis set*, and the overlap matrix S. In a first step, the MO coefficients are transformed from the non-orthogonal basis to the orthogonal set of atomic orbitals by the Löwdin orthogonalization,

$$C_0^{'} = S^{1/2}C_0, \tag{5}$$

where $S^{1/2}$ results from the symmetric decomposition $S = S^{1/2}S^{1/2}$. The orthogonalized coefficients $C^{'}$ can then be used to recover the desired static Hamiltonian from the one-electron energies ε:

$$H_0 = C_0^{'}\varepsilon(C_0^{'})^{\dagger}, \tag{6}$$

where $(C_0^{'})^{\dagger} = (C_0^{'})^{-1}$, by virtue of the unitary character of the coefficient matrix.

In forming the time dependent term of the Hamiltonian matrix according to (3), given the appreciable size of the systems considered, we chose to employ the *static* multipole matrix M of the optimized donor-acceptor compound, produced along with the overlap matrix $S$and the initial MO coefficients C_0 in a preliminary static optimization calculation. More precisely, we considered the perturbation to act along the z-direction (the main orientation of the donor-acceptor complex) by including just the matrix M_z of the z-components of the molecular multipole moments, which, multiplied by the time-dependent factor, i.e. $E_0A(t)\sin(\omega t)M_z$, was subtracted element-by-element from the static Hamiltonian matrix H_0 to produce the time-dependent Hamiltonian matrix $H(t)$. The propagation matrix for the MO coefficients defined in relation (2) was efficiently generated by forming one triangle of a sequence of *symmetric real matrices* in packed vector-storage mode: $[I + H^2]$, $[I + H^2]^{1/2}$ (by a modified Choleski decomposition), $[I + H^2]^{-1/2}$ (as a symmetric inverse), and, finally, $[I + H^2]^{-1}$ (as square of the previous). To ensure the physical correctness of the overall propagation algorithm, we monitored at each time step the total electronic population (with marginal deviations of less than 10^{-4} e). We found this to be equivalent to checking the propagator's unitarity, and computationally more convenient. In addition, we also checked periodically the norm of the matrix $[I + H^2][I + H^2]^{-1}$.

As suggested by Acocella et al. [14] and Höfinger et al. [15], the initial electronic structure of the donor-acceptor complex can be conceived as a superposition of separate, non-interacting donor and acceptor states. Technically, the optimized geometric configuration of the complex is split into separate donor and acceptor configurations, which are subject to single-point calculations providing the MO coefficients, C_D and C_A, relative to the non-orthogonal basis set for each molecule individually. The orthogonalized MO coefficients of the donor, $C_D^{'} = S_D^{1/2}C_D$, and acceptor, $C_A^{'} = S_A^{1/2}C_A$, are used as blocks forming the initial MO coefficient matrix for the entire donor-acceptor complex:

$$C^{'}(t = 0) = \begin{pmatrix} C_D^{'} \\ C_A^{'} \end{pmatrix} \tag{7}$$

The ET is directly related to the change of electronic populations on the various MOs involved, and in terms of orthogonalized MO coefficients, the commonly used Löwdin population analysis can be conveniently employed [23]:

$$P = C'(C')^{\dagger}. \tag{8}$$

The formalism described above was implemented in a highly parallelized computer code (*Quest*), and was used throughout to perform the reported ET calculations.

3. Results and discussion

Sampling the space of relative donor-acceptor positions for equilibrium configurations is a tedious task for a compound involving van der Waals interactions, due to the presence of vast quasi-equipotential regions, leading to extremely slow convergence of any first-principles optimization approach. This behavior was plainly apparent even for a relatively small system, with barely 125 atoms, such as the considered donor-acceptor complex, composed of Tris[4-(2-thienyl)phenyl]amine ($C_{30}H_{21}NS_3$) as donor and C_{70} as acceptor (Fig. 1a and b) [2,24].

Using the PBEPBE exchange–correlation functional in conjunction

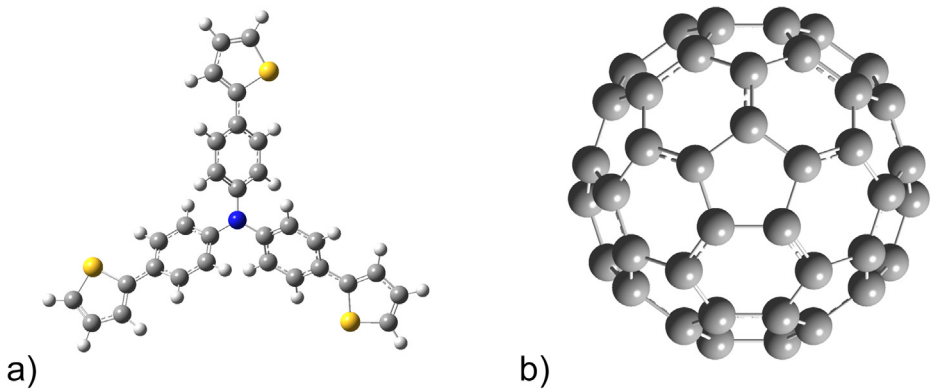

Fig. 1. (a) Tris[4-(2-thienyl)phenyl]amine ($C_{30}H_{21}NS_3$) donor; (b) C_{70} acceptor.

with the 6-31G* basis set for the geometry optimizations proved to be a reasonable choice, ensuring both a satisfying level of accuracy and requiring an acceptable amount of computational resources. Obviously, a dispersion-improved exchange–correlation functional and a superior basis set with diffuse functions would have been desirable, however, they dramatically increase the computational effort and will be discussed in a forthcoming publication. All static quantum mechanical calculations were performed using the Gaussian 09 program suite [25], with default convergence criteria.

Five representative initial donor-acceptor configurations (further on denoted by A through E) were considered, with the donor's central NC_3-group placed at a distance of 4 Å, parallel and centered over a particular pentagon or hexagon of the acceptor. As expected, the optimizations of these weakly-bonded complexes (started with the separately optimized donor and acceptor) converged extremely slowly and the resulted geometry configurations are shown in Fig. 2. It is noteworthy that the equilibrium donor-acceptor distances only changed within 0.2 Å, with an obvious shift of the projection of the donor's N atom towards the C-atom vertices of the acceptor's facing pentagon/hexagon (as illustrated in Fig. 3).

Subsequent to optimization, in order to obtain the detailed data needed for initiating the time evolution formalism (as explained in the methodology section), we performed for each configuration (A-E) three single-point calculations: one for the entire donor-acceptor complex, and two for the separate donor and acceptor, however not in their own equilibrium configurations, but in their distorted geometries within the complex.

The relevant electronic structure data obtained are summarized in Table 1. As can be judged from the close agreement of the HOMO, LUMO, and HOMO-LUMO gap values, the electronic structures of the five configurations are quite similar. Moreover, the total energy of all configurations coincides up to 7 significant digits, amounting to −5067.370 a.u. In relative terms, the deviations ΔE_{tot} of the total energies relative to configuration A can be seen to not exceed 0.013 eV, being thus over 30 times lower than the band gap.

Reflecting the true donor-acceptor character of the optimized complexes, the HOMO level of the separated donor fairly corresponds to the HOMO level of the entire compound, while the LUMO level of the separated acceptor agrees well with the LUMO level of the complex (as indicated in Table 1). The HOMO and LUMO orbitals for the donor, acceptor, and donor-acceptor complex corresponding to configuration C are depicted in Fig. 3. It can be noted that the HOMO orbital of the complex is completely localized on the donor fragment, whereas the LUMO orbital, on the acceptor fragment.

Knowing the excited electronic structure is very important for finding optimal conditions for the absorption of the electromagnetic

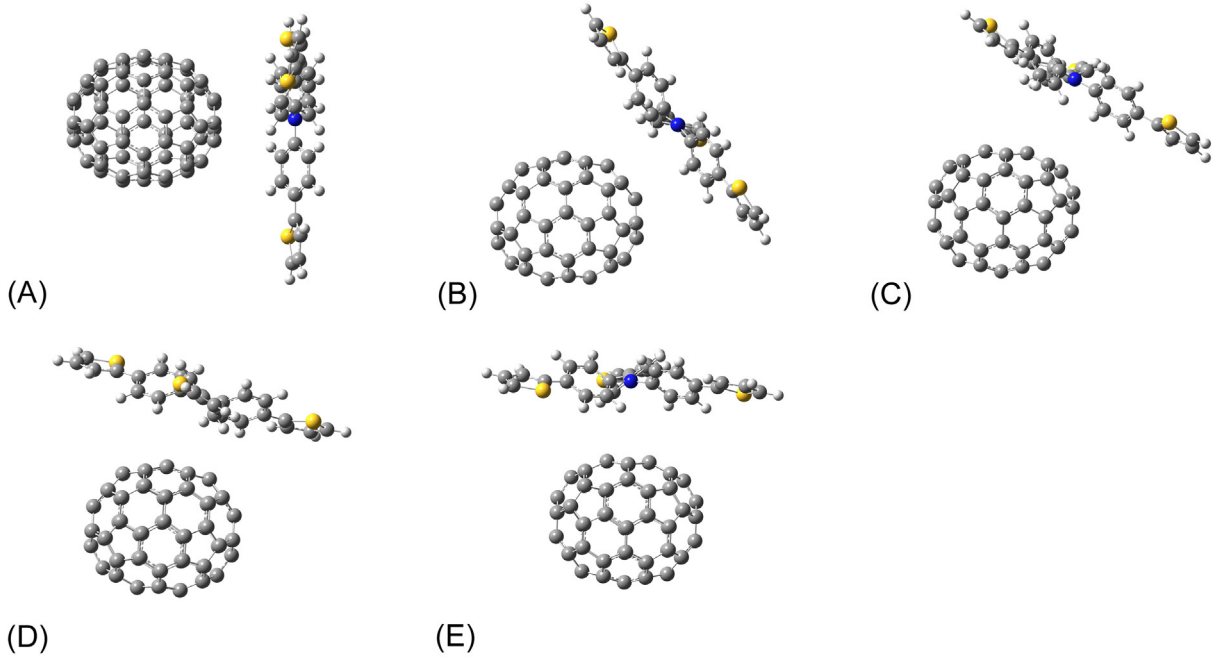

Fig. 2. Equilibrium configurations of the donor-acceptor complex.

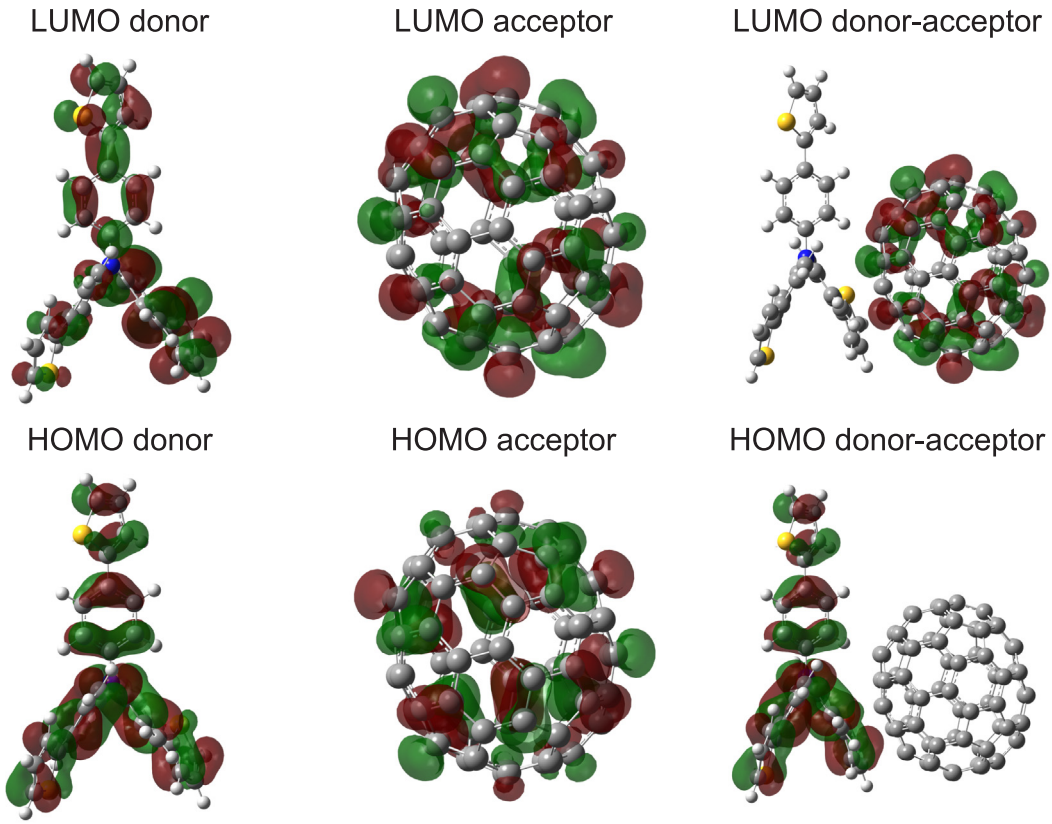

Fig. 3. HOMO and LUMO orbitals of the donor, acceptor and configuration C of the donor-acceptor complex.

Table 1
HOMO, LUMO, and gap energies (in eV) for configurations A-E of the donor-acceptor complex (DA), as well as for the separate donor (D) and acceptor (A) fragments. ΔE_{tot} represents the deviation of the total energy from the one of configuration A.

Config.	ΔE_{tot}		HOMO	LUMO	Gap
		D	−4.202	−1.888	2.314
A	0.000	A	−5.496	−3.790	1.706
		DA	−4.204	−3.767	0.437
		D	−4.202	−1.886	2.316
B	0.007	A	−5.496	−3.790	1.706
		DA	−4.200	−3.771	0.429
		D	−4.201	−1.888	2.313
C	−0.013	A	−5.496	−3.790	1.706
		DA	−4.194	−3.776	0.418
		D	−4.202	−1.887	2.315
D	−0.008	A	−3.791	−5.496	−1.705
		DA	−4.193	−3.776	0.417
		D	−4.200	−1.894	2.306
E	−0.005	A	−5.497	−3.791	1.706
		DA	−4.196	−3.772	0.424

radiation. Along this line, the time-dependent DFT calculation of the first five electronic excited states was performed, using the same exchange–correlation functional and basis set as in the geometry optimizations. The TDDFT calculations for the equilibrium geometry of the donor fragment in the C configuration yielded efficient absorption for the S_1 (472 nm) and S_2 (469 nm) excited electronic states.

The quantum evolution calculations were performed for a standard time span of 20 fs, using a time step of $2.5{\cdot}10^{-2}$ fs. In the absence of any perturbing pulse, the electronic populations on the donor and acceptor feature idle oscillations about their nominal static values (256 and 420, respectively), not exceeding 0.03 in amplitude. Irrespective of the donor-acceptor configuration, the oscillation frequency is typically about 2 PHz (corresponding to a wavelength of approximately 150 nm in the UV-C domain), which was taken as a reference.

In the actual ET calculations, we excited the donor-acceptor complex with Gaussian pulses of four frequency-duration combinations: P0: $\nu = 0.63$ PHz (or 475 nm) and $\tau = 5$ fs (close to the resonant $S_0 \rightarrow S_1$ electronic transition in the donor fragment), P1: $\nu = 1$ PHz (or 300 nm) and $\tau = 5$ fs, P2: $\nu = 2$ PHz (or 150 nm) and $\tau = 2.5$ fs, and P3: $\nu = 2$ PHz and $\tau = 5$ fs. The solar irradiance I at the ground level can be seen in Fig. 1 of [26] to reach values as high as 0.5 W/m^2/nm at the high-wavelength end of the UV region, corresponding to electric field strengths of about 19 V/m ($E_0 = \sqrt{2I/c\varepsilon_0}$), i.e. significantly higher than the one we used. Yet, the average irradiance over the interval between 225 and 375 nm barely reaches 0.08 V/m, corresponding to about 5 V/m. Accordingly, we performed calculations with $E_0 = 1$, 2, and 5 V/m, assuming less than perfect radiation absorption. As a matter of fact, under otherwise similar conditions, we found maximal ET for $E_0 = 1$ V/m.

Defining the ET by the difference between the instantaneous electron population and the nominal static number of electrons for each of the separate donor/acceptor moieties, Fig. 4 presents the corresponding time evolution upon applying pulse P1 to the donor-acceptor configurations A-E. In all five cases, the ET for the donor and acceptor can be seen to be of opposite sign and to perfectly compensate each other.

After a transitory inverse ET within the first few pulse cycles, the expected ET from donor to acceptor sets in, and is maintained even after the pulse extinction. For the pulse P1, the maximum ET is seen to amount for all donor-acceptor configurations to approximately 2 e, which is a reasonable value from an experimental perspective. Configuration C, seen to stand out by the highest final ET and the shortest onset, is employed in the following argumentation.

Considering pulses P2 and P3, with the frequency (2 PHz) in the identified resonant range of the donor-acceptor complex, the time evolution profiles plotted in Fig. 5 for configuration C show an

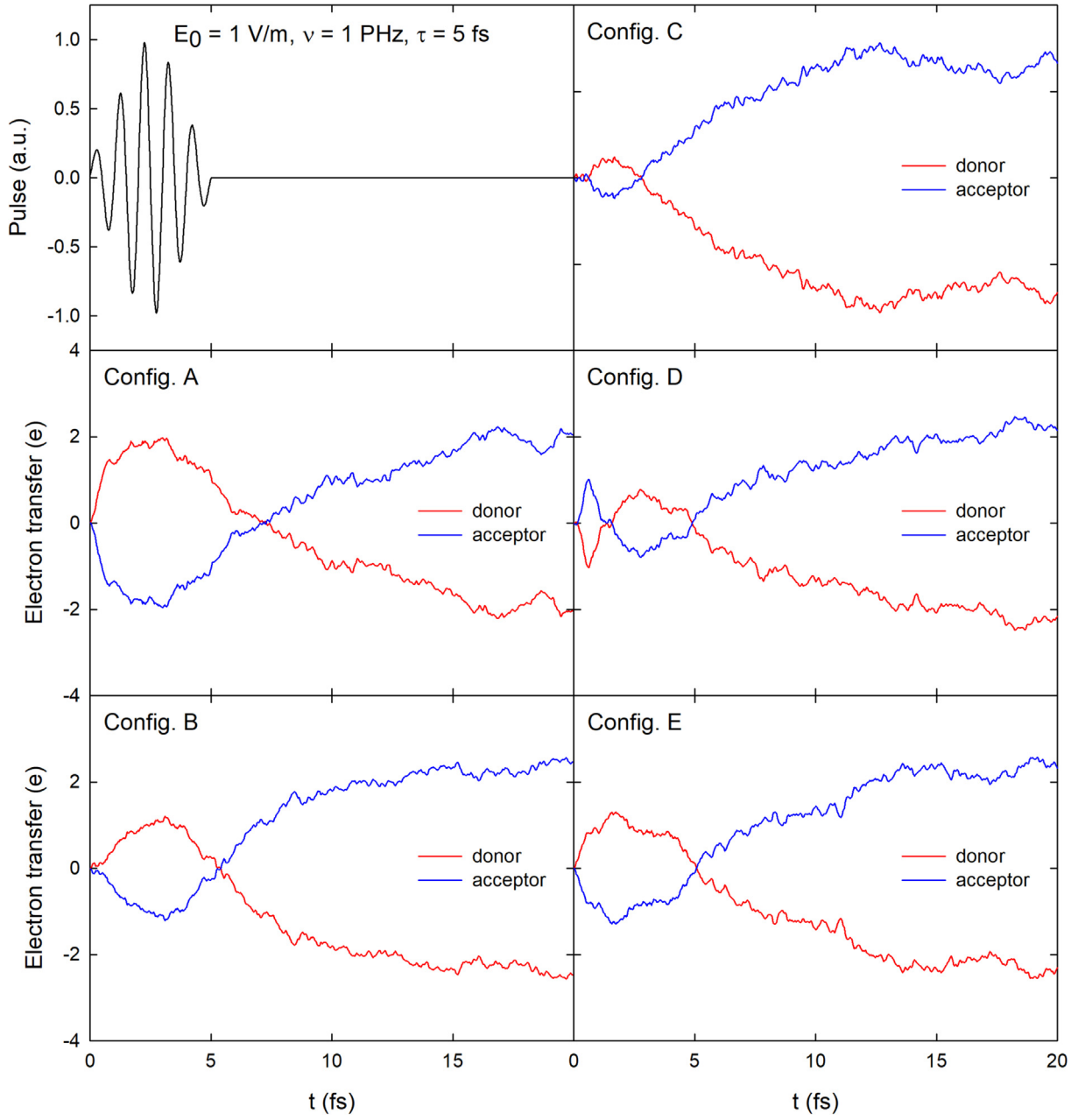

Fig. 4. Electron transfer for the five considered donor-acceptor configurations (A-E) under the influence of a pulse of electric field $E_0 = 1$ V/m, frequency $\nu = 1$ PHz, and duration$\tau = 5$ fs.

increased ET, with almost doubled maximum value for P3 (about 4 e). Indeed, as expected, besides using a frequency in the resonant range, doubling the pulse duration significantly contributes to the efficiency of the ET, and this is obviously due to the increased energy input.

With a view to a more quantitative comparison of the different setups, rather than characterizing the ET by the maximum value, we used the average ET over the whole simulated time span of 20 fs. Table 2 collects the results, and, for all configurations, the average transfer is seen to increase both for the frequency in the resonant range (2 PHz) and the longer pulse duration (5 fs), reaching the maximum values for pulse P3. While, for pulse P1, configuration C is the one showing the largest average ET (1.842 e), for pulse P3, the highest ET efficiency is reached for configuration D (2.691 e). It can also be noted that for pulse P3, configuration B stands out, showing the lowest ET (1.699 e), in contrast with the rest of the configurations having ET values over 2.1 e.

The particular case of P0 would mean the lowest energy (highest frequency) regime to which one can still observe the excitation of the donor fragment caused by the external field. At the same time, it can also be seen that the amount of the electron transfer differs the most for this P0 case, starting from a slightly invers electron transfer (-0.285*e*) in case A to a strong transfer (+2.198*e*) in case D. In other words, the structural differences between the A-D complexes provide the greatest differences in the electron transfer effects for the P0 type of excitation setup.

Given the practically similar static electronic structures of all five donor-acceptor configurations (as discussed above), the differences found in ET rather emphasize preferential geometric arrangements of the donor and acceptor in relation to the applied pulses.

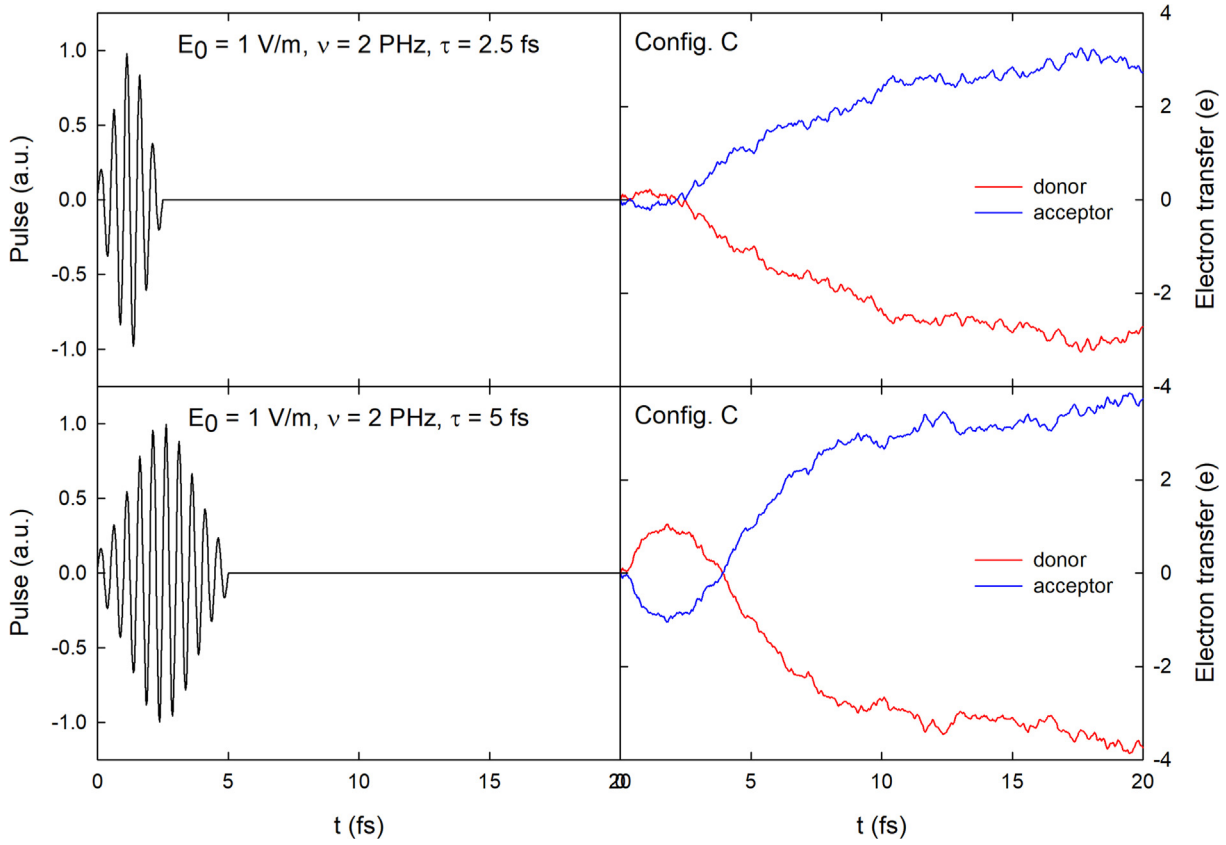

Fig. 5. Electron transfer for configuration C of the donor-acceptor complex, for Gaussian pulses of frequency 2 PHz and durations 2.5 fs and 5 fs, respectively.

Table 2
Average electron transfer (positive values mean transfer from donor to acceptor, while negative values imply reversed transfer) for configurations A-E of the donor-acceptor complex, for different frequencies ν and durations τ of the Gaussian pulse.

Config.	ν(PHz)	Electron transfer (e)	
		τ = 2.5 fs	τ = 5 fs
A	0.63		−0.285
	1.00		0.448
	2.00	1.131	2.218
B	0.63		1.517
	1.00		1.195
	2.00	1.052	1.699
C	0.63		1.132
	1.00		1.842
	2.00	1.893	2.124
D	0.63		2.198
	1.00		1.135
	2.00	2.260	2.691
E	0.63		0.124
	1.00		1.060
	2.00	1.087	2.250

4. Conclusions

Aiming to contribute to understanding the electron transfer processes occurring in donor-acceptor systems of relevance for photovoltaic applications, we performed detailed time-dependent quantum mechanical calculations of the electronic populations of complexes composed of the star-shaped molecule Tris[4-(2-thienyl)phenyl]amine ($C_{30}H_{21}NS_3$) as donor and the C_{70} fullerene as acceptor.

We considered several representative optimized donor-acceptor geometrical configurations, which turned out to have similar electronic structure, with the HOMO and LUMO orbitals completely localized on the donor and acceptor fragments, respectively. The corresponding static Hamiltonians and molecular orbitals were employed in conjunction with Gaussian pulses to construct perturbed Hamiltonians and initial states for a time evolution formalism based on Cayley's propagator.

The dynamics of the electronic populations (obtained by standard Löwdin analysis), clearly evidences an average electron transfer from donor to acceptor, typically amounting to about two electrons over a time span of 20 fs. The electron transfer efficiency is shown to increase both by pulse frequencies in the range of a resonance of the donor-acceptor complex and by increased pulse durations. The configurations yielding the highest and lowest electron transfers are identified, and the relevance of the geometrical arrangement is emphasized.

CRediT authorship contribution statement

Titus-Adrian Beu: Conceptualization, Investigation, Methodology, Formal analysis, Validation, Visualization, Writing - original draft, Supervision, Software. **Attila Bende:** Conceptualization, Formal analysis, Validation, Writing - review & editing. **Alex-Adrian Farcaş:** Investigation, Formal analysis.

Declaration of Competing Interest

The authors declare that they have no known competing financial interests or personal relationships that could have appeared to influence the work reported in this paper.

References

[1] Z. Zheng, N.R. Tummala, Y.-T. Fu, V. Coropceanu, J.-L. Brédas, ACS Appl Mater. Interfaces 9 (2017) 18095–18102.
[2] C.W. Tang, Appl. Phys. Lett. 48 (1986) 183.

[3] L. Bucher, N. Desbois, P.D. Harvey, G.D. Sharma, C.P. Gros, Solar RRL 1 (12) (2017) 1700127.
[4] S. Collavini, J.L. Delgado, Sustain Energy Fuels 2 (2018) 2480–2493.
[5] F. Wessendorf, B. Grimm, D.M. Guldi, A. Hirsch, J. Am. Chem. Soc. 132 (2010) 10786–10795.
[6] J. Kesters, P. Verstappen, M. Kelchtermans, L. Lutsen, D. Vanderzande, W. Maes, Adv. Energy Mater. 5 (2015) 1500218.
[7] R. Wang, R. Qu, C. Jing, Y. Zhai, Y. An, L. Shi, RSC Adv. 7 (2017) 10100.
[8] M. Hiramoto, Y. Shinmura, Organic Solar Cells, in: S. Kasap, P. Capper (Eds.), Springer Handbook of Electronic and Photonic Materials, Springer Handbooks. Springer, Cham, 2017.
[9] Y. Li, D. Qi, P. Song, F. Ma, Materials 8 (2015) 42–56.
[10] Y. Song, A. Schubert, X. Liu, S. Bhandari, S.R. Forrest, B.D. Dunietz, E. Geva, J.P. Ogilvie, J. Phys. Chem. Lett. 11 (6) (2020) 2203–2210.
[11] M.A. Izquierdo, R. Broer, R.W.A. Havenith, J. Phys. Chem. A 123 (6) (2019) 1233–1242.
[12] S. Joseph, M.K. Ravva, J.-L. Brédas, J. Phys. Chem. Lett. 8 (2017) 5171–5176.
[13] J.S. Graves, R.E. Allen, Phys. Rev. B 58 (1998) 13627–13633.
[14] A. Acocella, J.A. Garth, F. Zerbetto, J. Phys. Chem. B 114 (11) (2010) 4101–4106.
[15] S. Höfinger, A. Acocella, S.C. Pop, T. Narumi, K. Yasuoka, T. Beu, F. Zerbetto, J. Comput. Chem. 33 (29) (2012) 2351–2356.
[16] A. Acocella, S. Höfinger, E. Haunschmid, S.C. Pop, T. Narumi, K. Yasuoka, M. Yasui, F. Zerbetto, Phys. Chem. Chem. Phys. 20 (8) (2018) 5708–5720.
[17] C.J. Brabec, G. Zerza, G. Cerullo, S. De Silvestri, S. Luzzatti, J.C. Hummelen, N.S. Sariciftci, Chem. Phys. Lett. 340 (3–4) (2001) 232–236.
[18] Y. He, H.-Y. Chen, J. Hou, Y. Li, J. Am. Chem. Soc. 132 (4) (2010) 1377–1382.
[19] M.M. Wienk, J.M. Kroon, W.J.H. Verhees, J. Knol, J.C. Hummelen, P.A. van Hal, R, A.J. Janssen, Angew. Chem., Int. Ed. 42 (29) (2003) 3371–3375.
[20] R.E. Allen, Phys. Rev. B 50 (1994) 18629.
[21] A. Szabo, N.S. Ostlund, Modern quantum chemistry, Introduction to Advanced Electronic Structure Theory, Dover Publications, New York, 1982.
[22] F. Jensen, Introduction to Computational Chemistry, John Wiley & Sons, Sussex, 2007.
[23] P.O. Löwdin, J. Chem. Phys. 18 (1950) 365.
[24] S.H. Park, A. Roy, S. Beaupré, S. Cho, N. Coates, J.S. Moon, D. Moses, M. Leclerc, K. Lee, A.J. Heeger, Nat. Photon. 3 (5) (2009) 297–302.
[25] M.J. Frisch, G.W. Trucks, H.B. Schlegel, G.E. Scuseria, M.A. Robb, J.R. Cheeseman, J.A. Montgomery, Jr., T. Vreven, K.N. Kudin, J.C. Burant, J.M. Millam, S.S. Iyengar, J. Tomasi, V. Barone, B. Mennucci, M. Cossi, G. Scalmani, N. Rega, G.A. Petersson, H. Nakatsuji, M. Hada, M. Ehara, K. Toyota, R. Fukuda, J. Hasegawa, M. Ishida, T. Nakajima, Y. Honda, O. Kitao, H. Nakai, M. Klene, X. Li, J.E. Knox, H.P. Hratchian, J.B. Cross, C. Adamo, J. Jaramillo, R. Gomperts, R.E. Stratmann, O. Yazyev, A.J. Austin, R. Cammi, C. Pomelli, J.W. Ochterski, P.Y. Ayala, K. Morokuma, G.A. Voth, P. Salvador, J.J. Dannenberg, V.G. Zakrzewski, S. Dapprich, A.D. Daniels, M.C. Strain, O. Farkas, D.K. Malick, A.D. Rabuck, K. Raghavachari, J.B. Foresman, J.V. Ortiz, Q. Cui, A.G. Baboul, S. Clifford, J. Cioslowski, B.B. Stefanov, G. Liu, A. Liashenko, P. Piskorz, I. Komaromi, R.L. Martin, D.J. Fox, T. Keith, M.A. Al-Laham, C.Y. Peng, A. Nanayakkara, M. Challacombe, P.M.W. Gill, B. Johnson, W. Chen, M. W. Wong, C. Gonzalez, and J.A. Pople, Gaussian 09, Revision A. 01, Gaussian Inc., Pittsburgh, PA, 2013.
[26] K. Ranabhat, L. Patrikeev, A.A. Revina, K. Andrianov, V. Lapshinsky, E. Sofronova, OA, J. Appl. Eng. Sci. 14 (4) (2016) 481–491.